Published in final edited form as:
Histochem Cell Biol. 2010 April ; 133(4): 405–415. doi:10.1007/s00418-010-0680-3.

Tissue Stretch Induces Nuclear Remodeling in Connective Tissue Fibroblasts

Helene M. Langevin[*,‖], **Kirsten N. Storch**[*], **Robert R. Snapp**[§], **Nicole A. Bouffard**[*], **Gary J. Badger**[¶], **Alan K. Howe**[#], and **Douglas J. Taatjes**[†]

[*]Department of Neurology, University of Vermont College of Medicine 89 Beaumont Ave. Burlington, VT 05405, USA

[‖] Department of Orthopaedics & Rehabilitation, University of Vermont College of Medicine 89 Beaumont Ave. Burlington, VT 05405, USA

[§] Department of Computer Science, University of Vermont College of Medicine 89 Beaumont Ave. Burlington, VT 05405, USA

[¶] Department of Medical Biostatistics, University of Vermont College of Medicine 89 Beaumont Ave. Burlington, VT 05405, USA

[#] Department of Pharmacology, Vermont Cancer Center, University of Vermont College of Medicine 89 Beaumont Ave. Burlington, VT 05405, USA

[†]Department of Pathology University of Vermont College of Medicine 89 Beaumont Ave. Burlington, VT 05405, USA

Abstract

Studies in cultured cells have shown that nuclear shape is an important factor influencing nuclear function, and that mechanical forces applied to the cell can directly affect nuclear shape. In a previous study, we demonstrated that stretching of whole mouse subcutaneous tissue causes dynamic cytoskeletal remodeling with perinuclear redistribution of α-actin in fibroblasts within the tissue. We have further shown that the nuclei of these fibroblasts have deep invaginations containing α-actin. In the current study, we hypothesized that tissue stretch would cause nuclear remodeling with a reduced amount of nuclear invagination, measurable as a change in nuclear concavity. Subcutaneous areolar connective tissue samples were excised from 28 mice and randomized to either tissue stretch or no stretch for 30 minutes, then examined with histochemistry and confocal microscopy. In stretched tissue (vs. non-stretched), fibroblast nuclei had a larger cross sectional area ($p<.001$), smaller thickness ($p<.03$) in the plane of the tissue, and smaller relative concavity ($p<.005$) indicating an increase in nuclear convexity. The stretch-induced loss of invaginations may have important influences on gene expression, RNA trafficking and/or cell differentiation.

Keywords

Cytoskeleton; subcutaneous; nucleus; mechanotransduction; invagination

Corresponding Author: Helene M. Langevin, Department of Neurology, University of Vermont, helene.langevin@uvm.edu, tel: 802-656-1001, fax: 802-656-8704.

Disclosure: Helene M. Langevin is a partner of Stromatec, Inc.

Introduction

The cell nucleus is increasingly recognized as a highly dynamic organelle whose function is intrinsically linked to its structural organization (Dundr and Misteli, 2001). Nuclear shape has been shown to influence fundamental aspects of nuclear function including chromatin remodeling and gene transcription (Dalby et al., 2007; Itano et al., 2003; Lammerding et al., 2004; Thomas et al., 2002). One of the most dramatic changes in nuclear shape is the folding and unfolding of nuclear invaginations. These structures are thought to play a role in cell differentiation as well as chromatin organization, nucleocytoplasmic transport, calcium signaling and RNA trafficking (Abe et al., 2004; Bloom et al., 1996; Echevarria et al., 2003; Fricker et al., 1997; Johnson et al., 2003). There is also evidence that the commitment of a cell to proliferation or differentiation can be influenced by the overall shape of the cell, in addition to the shape of its nucleus (Ben-Ze'ev et al., 1980; McBeath et al., 2004). A proposed mechanism underlying this phenomenon is that cell shape affects nuclear shape which in turn affects chromatin remodeling and gene expression (Ingber et al., 1987; Maniotis et al., 1997).

Studies in cultured cells and whole tissue have shown that the shape, position and orientation of the nucleus as well as the organization of the nuclear lamina can be influenced by mechanical forces applied to the cell (Bloom et al., 1996; Flaherty et al., 1972; Gieni and Hendzel, 2007; Guilak, 1995; Hu et al., 2005; Huang et al., 2007; Maniotis et al., 1997; Philip and Dahl, 2008). Changes in nuclear shape in response to an applied force can results from passive viscoelastic deformation (Guilak et al., 2000; Rowat et al., 2006; Vaziri and Mofrad, 2007) as well as active cytoskeletally-mediated structural remodeling (Deguchi et al., 2005). We have previously shown that the nuclei of fibroblasts within mouse subcutaneous “loose” areolar connective tissue have deep nuclear invaginations containing cytoplasm that are associated with concavity of the nuclear surface (Storch et al., 2007). We also have shown that stretching of the whole tissue causes these fibroblasts to respond rapidly (i.e. within minutes) with extensive cell spreading, lamellipodia formation and perinuclear actin redistribution (Langevin et al., 2005; Storch et al., 2007). The current study was designed to test the hypothesis that tissue stretch results in nuclear remodeling measurable as a change in the degree of nuclear concavity.

Materials and Methods

The experimental protocols used in these experiments were approved by the University of Vermont IACUC Committee. Two complementary groups of experiments were performed using different tissue fixation methods: 3% paraformaldehyde (PFA) was used in experiments examining nuclear concavity, while 95% ethanol was used in experiments examining cell cross sectional area, nuclear orientation and nuclear eccentricity. Although both fixatives yielded similar results with respect to the basic difference in nuclear shape between stretched and non-stretched tissue (Figure 1), each fixative had distinct advantages and limitations: PFA produced less tissue shrinking and better preservation of nuclear morphological detail but did not allow preservation of tissue orientation. Ethanol fixation yielded optimal visualization and measurement of cell body shape (Langevin et al., 2004) and allowed preservation of tissue orientation during tissue dissection (see method below) but produced more tissue shrinking (nuclear cross sectional area was ~30% smaller with ethanol compared with PFA fixation).

Effect of tissue stretch on nuclear cross sectional area and concavity

We performed a set of experiments in which we examined the effect of tissue stretch on nuclear shape in high magnification confocal microscopy images. Tissue samples from 28 mice were excised and randomized to either stretch (n = 14) or no stretch (n = 14) ex vivo for 30 minutes followed by tissue fixation in 3% PFA and staining of the nucleus with DAPI.

Nuclear cross sectional area, orientation and eccentricity with immediate (2 minutes) vs. sustained (30 minutes) stretch, and after the release of stretch

To investigate whether the observed stretch-induced changes in nuclear shape are primarily passive (either from direct stretching of the nucleus or compression of the nucleus from thinning of the stretched tissue), as opposed to active remodeling, we measured nuclear cross sectional area, eccentricity and orientation after 2 minutes (N=3 mice) and 30 minutes (N=3 mice) of stretch *ex vivo*, as well as in tissue stretched for 30 minutes, then released for 2 minutes (N=3 mice) and 10 minutes (N=3 mice). Samples were fixed in 95% ethanol for 1 hour. Subcutaneous tissue samples were dissected on three sides and separated from the subcutaneous muscle, leaving a partially attached tissue flap that was allowed to rehydrate in PBS containing 1% BSA overnight. A glass slide was then placed under the sample and the fourth side was cut while preserving the orientation of samples relative to the direction of stretch. Fixation was followed by staining with DAPI.

Effect of pharmacological inhibitor

10 μM Rho kinase inhibitor Y27632 (BioMol, Philadelphia, PA) was used to investigate the role of Rho-dependent cytoskeletal remodeling in stretch-induced change in nuclear shape. Tissue samples were cut in half then randomized to stretch vs. no stretch. Each sample was incubated for 10 minutes with the inhibitor, then stretched (or not stretched) for 30 minutes. Samples were then fixed in 3% PFA for 1 hour as above, then stained with DAPI.

Relationship between cell cross sectional area and nuclear cross sectional area

We examined the relationship between cell cross sectional area and nuclear cross-sectional area in a set of confocal laser microscopy images obtained in a previously published study in which 23 male C57Black6 mice weighing 19-21 g were randomized to either stretch or no stretch for 10, 60 or 120 minutes *ex vivo* (Langevin et al., 2005). Tissue stretch was followed by tissue fixation in 95% ethanol and histochemical staining with phalloidin for visualization of cell bodies and SYTOX green nucleic acid stain for visualization of the nucleus. Cell and nuclear cross sectional area were measured as described below.

Stretched and non-stretched subcutaneous tissue sample preparation

In all experiments, tissue samples were harvested from the abdomen immediately after death in C57BL/6 male mice (19-21g). Whole skin flaps (8 cm × 3 cm) containing dermis, subcutaneous muscle and subcutaneous tissue were dissected away from the abdominal wall musculature, excised, and placed between stainless steel grips submerged in HEPES-physiological saline solution (HEPES-PSS) (141.8 mM NaCl, 4.7 mM KCl, 1.7 mM $MgSO_4$, 0.39 mM EDTA, 2.8 mM $CaCl_2$, 10.0 mM HEPES, 1.2 mM KH_2PO_4, 5.0 mM glucose, pH 7.4) at 37°C as previously described (Langevin et al., 2005). Tissue grips were connected to a 500 g capacity strain gauge transducer. Samples randomized to stretch were elongated at a rate of 1 mm/sec by advancing a micrometer connected to the distal tissue grip until a load of 0.02 N (corresponding to 15-25% tissue strain relative to non-stretched length) was registered, then maintained at that length for the prescribed incubation time. Non-stretched samples were incubated in grips for 30 minutes at the length corresponding to the length of the tissue laying flat. At the end of incubation, samples were fixed in 3% PBS or 95% ethanol at the stretched (or unstretched) length. After fixation, three samples of areolar connective tissue were dissected for each animal. Samples located between the superficial (subcutaneous) fascia and the deep (muscular) fascia were dissected (sample dimensions 20-30 mm in width, 60-80 mm in length and 20-50 μm in thickness), mounted on glass slides and rinsed in PBS/1.0% BSA/0.1% Triton × 100.

Histochemical and immunohistochemical staining

Unless stated otherwise, histochemical staining of the nucleus was performed with 4′,6-diamidino-2-phenylindole, dihydrochloride (DAPI) nucleic acid stain (Invitrogen, Carlsbad, CA) at a dilution of 1:1000 for five minutes at room temperature. Samples were counterstained with Texas Red conjugated Phalloidin, a specific stain for polymerized actin, (Invitrogen, Carlsbad, CA) at a 1:25 dilution for 40 minutes at 4°C for visualization of cell bodies. A subset of PFA-fixed samples were also stained for α-actin using indirect immunohistochemistry. Samples were first incubated with a mouse monoclonal anti-α-smooth muscle actin primary antibody (Sigma, St. Louis, MO) at 1:100 dilution followed by an Alexa 488-conjugated secondary goat anti-mouse antibody (Invitrogen Corporation, Carlsbad, CA) at 1:200 dilution as previously described (Langevin et al., 2006). To reduce background staining resulting from using a mouse primary antibody, samples were incubated with Mouse-On-Mouse (M.O.M) blocking reagents (Vector Laboratories, Burlingame, CA) according to the manufacturers' directions. Samples were overlaid with a glass coverslip using 50% glycerol in PBS with 1% N-propylgallate as a mounting medium.

Confocal scanning laser microscopy

Tissue samples were imaged with a Zeiss LSM 510 META confocal scanning laser microscope. Four to six fields per sample were first imaged at 63× by an operator unaware of the study condition (stretch vs. no stretch). One to two cells per field were then imaged at higher magnification using a PlanApochromat 100× (1.4 N.A.) oil immersion lens, focusing directly on the nuclei using a zoom factor of two times. Thus, a total of 12-15 cells were imaged at both magnifications per animal. Z-stacks were acquired such that the entire thickness of each nucleus was captured. Each optical section had an optical thickness of 0.7 μm for all laser lines and a 0.33 μm inter image interval.

Morphometric analysis

Nuclear cross sectional area and relative concavity—The shape of each nucleus, projected onto the plane of the tissue, was measured in relation to its convex hull, the smallest convex region that encloses the nuclear projection. (Recall that a region R is said to be convex if and only if every line segment XY lies completely within R for every X and Y in R.) Letting *a* denote the nuclear cross sectional area (defined as the area of the nuclear projection onto the plane of the tissue), and *h* the area of its convex hull, we define the area of the deficit as $d=h-a$, which estimates the sum of the invaginated regions. We then define the relative concavity as $c=d/h$. Consequently, a convex nucleus --- one without invaginations or indentations --- results in a relative concavity of 0.

It is necessary to preprocess each image stack in a consistent manner before the relative concavity can be measured. Image stacks were imported into a custom made image analysis program. The nuclear cross sectional area was estimated from the 2-d projections of the image stacks onto the plane of the tissue. Projected images were thresholded for DAPI by an investigator unaware of the study condition. For each image a threshold level was chosen that optimally revealed the nuclear boundary in the presence of image noise. A closure operation was then performed in order to fill isolated interior pixels that were below the threshold (Figure 2A). Each active pixel was then assigned to a connected component following a sequential labeling algorithm (Horn, 1986). The convex hull for the largest connected component was then computed using a randomized incremental algorithm (Berg, 1997). Initially, three active pixels were chosen, at random, from the largest component to form a nondegenerate triangle (having a nonzero area), defining the vertices of the initial “convex polygon”. One by one, each remaining active pixel in the component was chosen in random order. Pixels falling within the incremental convex polygon were ignored. Whenever a pixel fell outside of the incremental convex polygon it was added as a new vertex, replacing the vertices that fall within the interior

of the enlarged convex polygon. (Figure 2 A,B). Letting a denote the area of the largest component, and *h*, the area of its convex hull, we compute the relative concavity of the nuclear cross section as c = *(h – a)/h = d/h*. (Figure 2C). Measurably concave regions ranged from shallow depressions to deep intranuclear invaginations.

Nuclear thickness—For measurement of nuclear thickness, image stacks were imported into the image analysis software package MetaMorph (Molecular Devices, Downington, PA). Nuclear thickness was estimated by counting the number of individual optical sections in which a nucleus appeared, multiplied by the optical inter image interval (0.33 μm).

Nuclear volume—For measurement of nuclear volume, image stacks were imported into the analysis software package Volocity (Improvision, Lexington, MA) to calculate voxel based nuclear volume estimations. In this program, the images of nuclei were cropped by thresholding on DAPI staining. To account for variations in staining levels between samples, a threshold of average intensity +1.0σ was used to select the entire nucleus, then the "fill holes" option was chosen where objects less than 1 μm^3 in size were excluded to reduce noise.

Nuclear eccentricity and orientation

The elongation of each nuclear area is described in terms of the first and second central moments of the locations of the pixels from the corresponding connected component: the two-dimensional mean (μ) estimates the location of the nuclear center, while the 2×2 covariance matrix (S) describes the second-order spread about the center. Then the eigenvalues (λ_1, λ_2) and eigenvectors (v_1, v_2) of the covariance matrix (S) are computed algebraically, such that $Sv_i = \lambda_i v_i$, for $i = 1$, and 2, with $\lambda_1 \geq \lambda_2 \geq 0$. We define the orientation of the nucleus as the angle between the dominant eigenvector (v1) and the horizontal axis, and the eccentricity as the square root of the eigenvalue ratio, i.e., $\sqrt{\lambda_1 / \lambda_2}$ (Pratt, 1991).

Cell body cross sectional area

Cell body cross sectional area was measured in six fields per sample using MetaMorph software for morphometric analysis as previously described (Langevin et al., 2005).

Statistical Methods—Differences between stretched and non-stretched tissue with respect to nuclear outcome measures were evaluated using analyses of variance corresponding to a nested design. The replicate observations derived from the 8-12 cells examined per animal were considered a nested factor within mouse. The F-tests corresponding to testing differences between experimental conditions (i.e. stretch and no stretch) utilized across-animal variability within each condition (df = 26), not the variability associated with replicate cells within each animal, as the appropriate error term. Analyses were performed using SAS Version 8, PROC MIXED (SAS Institute, Cary, NC). Statistical significance was determined based on $\alpha = 0.05$.

In the additional analysis of data from previously published experiments, the relationship between cell cross-sectional area and nuclear cross-sectional area at different time points in stretched and non-stretched samples was examined using correlation analyses.

Results

Fibroblast nuclei within non-stretched areolar connective tissue were smaller and more concave compared with those in stretched tissue, which tended to be round or oval with a smooth circumference (Figure 3). Morphometric measurements showed that fibroblast nuclei in stretched tissue, compared with non-stretched tissue had significantly greater nuclear cross sectional area (mean ± SE 109 ± 3 μm^2 vs. 93 ± 3 μm^2, $F_{1,26}$=13.9, p = .001) (Figure 4A) and decreased thickness (3.28 ± 0.12 μm vs. 3.63 ± 0.09 μm, $F_{1,2\ 6}$= 5.4, p = .03) (Figure 4C).

Nuclear volume showed a trend similar to that of cross sectional area, i.e. became on average larger in stretched compared with non-stretched tissue but this difference was not statistically significant (365 ± 12 μm^3 vs. 333 ± 14 μm^3 $F_{1,26} = 4.2$, p= .05) (Figure 4B). Fibroblast nuclei within stretched tissue also were less concave, having a smaller relative concavity than the nuclei of non-stretched tissue (0.02 ± 0.0017 vs. 0.03 ± 0.002 for stretch and no stretch respectively, $F_{1,26} = 9.6$, p = .005) (Figure 4D).

There was no significant difference in cellular or nuclear cross sectional area between stretched and non-stretched tissue after 2 minutes of stretch (Figure 5). In tissue that was stretched for 30 minutes and then either released for 2 or 10 minutes, or not released, significant differences were observed between conditions for cell cross sectional area, but not nuclear cross sectional area ($F_{2,6}$=18.9, p<.003) (Figure 5). Cell cross sectional area was significantly reduced after 2 minutes (p=.003) and 10 minutes (p=.001) of release (Fisher's LSD). Although there was a trend toward decreased nuclear cross sectional area in released tissue, this did not reach statistical significance (p=.42 for 2 minutes and p=.07 for 10 minutes). There were no significant differences in nuclear orientation or eccentricity within the image plane in tissue stretched vs. non-stretched for 2 or 30 minutes (data not shown).

Nuclear cross-sectional area was generally moderately correlated with cell cross-sectional area in both stretched and non-stretched conditions at 10 minutes, 60 minutes and 120 minutes of incubation (illustrated for 120 minutes in Figure 6) suggesting that the stretch-induced change in cell shape may be related to the change in nuclear shape. This is further suggested by the observation that the pattern of α-actin changed both within and outside the nuclear domain in response to tissue stretch (Figures 7). In non-stretched tissue, α-actin was present throughout the cytoplasm as well as within deep nuclear invaginations (Figure 8) as previously reported (Storch et al., 2007). In contrast, in stretched tissue, α-actin immunoreactivity was redistributed predominantly around the nucleus and was not detectable within the nuclear domain (Figure 9). In order to further investigate a possible link between cytoskeletal and nuclear remodeling, we examined the shape of fibroblast nuclei in the presence of an inhibitor of Rho kinase, which regulates cytoskeletal actin bundle contractility (Burridge and Wennerberg, 2004;Ridley and Hall, 1992;Ridley et al., 1992). In the presence of the Rho kinase inhibitor, nuclei had a similar morphology with and without stretch (Figure 10). Mean±SE nuclear cross sectional area was 74.6±9.5 μ^2 with stretch and 77.4±5.4 μ^2 without stretch (based on N=11-14 cells per condition). This suggests that Rho- dependent cytoskeletal mechanisms are required for change in nuclear shape in response to tissue stretch.

Discussion

Stretching of connective tissue for 30 minutes caused a change in the shape of fibroblast nuclei which were wider, flatter and smoother (less concave) than those within non-stretched tissue. Our confocal images show that nuclei in non-stretched tissue had indentations ranging from small wrinkles to deep invaginations, all of which contributed to greater nuclear concavity (Figure 2). Tissue stretch was associated with both loss of deep invaginations, as well as superficial smoothing of the nuclear surface. The potential consequences of stretch-induced nuclear remodeling and loss of nuclear concavity are far reaching, since mounting evidence suggests that cell and nuclear shape can influence cell differentiation, chromatin structure, and histone acetylation (Chen et al., 1997;Dalby, 2005;Kim et al., 2005). Indeed, direct transmission of forces through the cytoplasmic and nuclear cytoskeleton via changes in cell and nuclear shape has been proposed as a source of specific coupling between tissue mechanical forces and the genome (Gieni and Hendzel, 2007). In addition, because nuclear invaginations bring cytoplasmic space closer to the interior of nuclear domain, these structures are thought to be an important conduit for nucleocytoplasmic transport (Bourgeois et al., 1979;Dupuy-Coin et al., 1986).

The change in nuclear shape and smoothing of the nuclear surface could result from direct viscoelastic deformation (from in-plane tensile forces and/or perpendicular compressive forces due to thinning of the tissue during stretching) or could represent a more complex phenomenon involving active reorganization of nuclear structure in response to tissue stretch. Micropipette aspiration experiments on isolated nuclei have shown that the nucleus reversibly deforms within seconds in response to a direct mechanical input (Guilak et al., 2000; Rowat et al., 2006; Vaziri and Mofrad, 2007). Recent rheological models based on soft glassy materials also suggest that nuclear stiffness can continue to change over longer time scales in response to mechanical deformation, and cytoskeletal remodeling has been suggested as a possible explanation for this type of biomechanical behavior (Dahl et al., 2005; Mandadapu et al., 2008). In a study of cartilage compressed for 30 minutes ex vivo, chondrocyte nuclei became flatter in response to tissue compression and this effect was inhibited by pretreatment with cytochalasin-D, suggesting that the actin cytoskeleton plays a role linking extracellular matrix compression and nuclear deformation (Guilak, 1995). In cultured endothelial cells, prolonged shear stress for 24 hours was shown to cause nuclear morphological and stiffness changes that persisted after isolation of the nuclei and were also prevented by cytochalasin-D, again suggesting structural remodeling (Deguchi et al., 2005). In the current study, the delayed onset of the change in nuclear morphology (more than 2 minutes) and the persistence of morphological changes after the release of tissue stretch suggest that the changes in nuclear shape observed in this study involve structural remodeling, rather than direct stretching or compression of the nuclei. The lack of change in nuclear eccentricity or orientation further suggests that the changes in nuclear shape observed in this study are not the direct result of tissue stretching. The change in cell shape and redistribution of perinuclear actin observed in response to tissue stretch shows that extensive cytoskeletal reorganization is taking place in response to tissue stretch. The lack of stretch-induced change in nuclear shape in the presence of Rho kinase inhibition further suggests that actin-based cytoskeletal mechanisms are involved in nuclear remodeling in response to tissue stretch.

A potential limitation of our study is that analyzing confocal image data in two dimensions may have underestimated nuclear concavity oriented perpendicular to the tissue that would not be visible in a two dimensional image stack projection. It is possible that out-of-plane changes in cell and nuclear orientation occur in response to mechanical forces (i.e., the cell and nucleus could rotate relative to the plane of the tissue or the nucleus could rotate relative to a more stationary cell body) (Gieni and Hendzel, 2007). We however consider it unlikely that differences in nuclear shape and relative concavity between stretched and non-stretched tissue were entirely due to rotation of nuclear invaginations out of the tissue plane. Because the nuclei of the fibroblasts are shaped like disks, we would expect that the aspect ratio (defined as the nuclear thickness divided by the square root of the nuclear cross sectional area) would increase as a result of rotation out of the tissue plane. However, the mean ± SE aspect ratio was 0.39 ± 0.014 for non-stretched tissue and 0.32 ± 0.016 for stretched tissue. This decrease in nuclear aspect ratio with stretch strongly suggests that nuclear deformation predominated over nuclear rotation.

In summary, stretching of whole mouse subcutaneous tissue resulted in a change in fibroblast nuclear shape with a loss of nuclear concavity. These results in whole tissue support a growing literature indicating that the mechanical environment of the cell has a profound influence on the cell nucleus.

Acknowledgments

The authors thank Drs. Nicholas Heintz and William C. Eanrshaw for helpful discussions. This work was funded by the National Institutes of Health Center for Complementary and Alternative Medicine research Grant RO1-AT01121 and by National Institutes of Health Grant P20 RR16435 from the Center of Biomedical Research Excellence Program of the National Center for Research Resources. Its contents are solely the responsibility of the authors and do not

necessarily represent the official views of the National Center for Complementary and Alternative Medicine, National Institutes of Health.

References

Abe T, Takano K, Suzuki A, Shimada Y, Inagaki M, Sato N, Obinata T, Endo T. Myocyte differentiation generates nuclear invaginations traversed by myofibrils associating with sarcomeric protein mRNAs. J Cell Sci 2004;117:6523–6534. [PubMed: 15572409]

Ben-Ze'ev A, Farmer SR, Penman S. Protein synthesis requires cell-surface contact while nuclear events respond to cell shape in anchorage-dependent fibroblasts. Cell 1980;21:365–372. [PubMed: 6157481]

Berg, Md. Computational geometry : algorithms and applications. Springer; Berlin; New York: 1997.

Bloom S, Lockard VG, Bloom M. Intermediate filament-mediated stretch-induced changes in chromatin: a hypothesis for growth initiation in cardiac myocytes. J Mol Cell Cardiol 1996;28:2123–2127. [PubMed: 8930807]

Bourgeois CA, Hemon D, Bouteille M. Structural relationship between the nucleolus and the nuclear envelope. J Ultrastruct Res 1979;68:328–340. [PubMed: 490761]

Burridge K, Wennerberg K. Rho and Rac take center stage. Cell 2004;116:167–179. [PubMed: 14744429]

Chen CS, Mrksich M, Huang S, Whitesides GM, Ingber DE. Geometric control of cell life and death. Science 1997;276:1425–1428. [PubMed: 9162012]

Dahl KN, Engler AJ, Pajerowski JD, Discher DE. Power-law rheology of isolated nuclei with deformation mapping of nuclear substructures. Biophys J 2005;89:2855–2864. [PubMed: 16055543]

Dalby MJ. Topographically induced direct cell mechanotransduction. Medical engineering & physics 2005;27:730–742. [PubMed: 15921949]

Dalby MJ, Gadegaard N, Herzyk P, Sutherland D, Agheli H, Wilkinson CD, Curtis AS. Nanomechanotransduction and interphase nuclear organization influence on genomic control. J Cell Biochem 2007;102:1234–1244. [PubMed: 17427951]

Deguchi S, Maeda K, Ohashi T, Sato M. Flow-induced hardening of endothelial nucleus as an intracellular stress-bearing organelle. J Biomech 2005;38:1751–1759. [PubMed: 16005465]

Dundr M, Misteli T. Functional architecture in the cell nucleus. Biochem J 2001;356:297–310. [PubMed: 11368755]

Dupuy-Coin AM, Moens P, Bouteille M. Three-dimensional analysis of given cell structures: nucleolus, nucleoskeleton and nuclear inclusions. Methods Achiev Exp Pathol 1986;12:1–25. [PubMed: 3007927]

Echevarria W, Leite MF, Guerra MT, Zipfel WR, Nathanson MH. Regulation of calcium signals in the nucleus by a nucleoplasmic reticulum. Nat Cell Biol 2003;5:440–446. [PubMed: 12717445]

Flaherty JT, Pierce JE, Ferrans VJ, Patel DJ, Tucker WK, Fry DL. Endothelial nuclear patterns in the canine arterial tree with particular reference to hemodynamic events. Circ Res 1972;30:23–33. [PubMed: 5007525]

Fricker M, Hollinshead M, White N, Vaux D. Interphase nuclei of many mammalian cell types contain deep, dynamic, tubular membrane-bound invaginations of the nuclear envelope. J Cell Biol 1997;136:531–544. [PubMed: 9024685]

Gieni RS, Hendzel MJ. Mechanotransduction from the ECM to the genome: Are the pieces now in place. J Cell Biochem. 2007

Guilak F. Compression-induced changes in the shape and volume of the chondrocyte nucleus. J Biomech 1995;28:1529–1541. [PubMed: 8666592]

Guilak F, Tedrow JR, Burgkart R. Viscoelastic properties of the cell nucleus. Biochem Biophys Res Commun 2000;269:781–786. [PubMed: 10720492]

Horn, B. Robot vision. MIT Press; McGraw-Hill; Cambridge, Mass. New York: 1986.

Hu S, Chen J, Butler JP, Wang N. Prestress mediates force propagation into the nucleus. Biochem Biophys Res Commun 2005;329:423–428. [PubMed: 15737604]

Huang HY, Liao J, Sacks MS. In-situ deformation of the aortic valve interstitial cell nucleus under diastolic loading. J Biomech Eng 2007;129:880–889. [PubMed: 18067392]

Ingber DE, Madri JA, Folkman J. Endothelial growth factors and extracellular matrix regulate DNA synthesis through modulation of cell and nuclear expansion. In Vitro Cell Dev Biol 1987;23:387–394. [PubMed: 2438264]

Itano N, Okamoto S, Zhang D, Lipton SA, Ruoslahti E. Cell spreading controls endoplasmic and nuclear calcium: a physical gene regulation pathway from the cell surface to the nucleus. Proc Natl Acad Sci U S A 2003;100:5181–5186. [PubMed: 12702768]

Johnson N, Krebs M, Boudreau R, Giorgi G, LeGros M, Larabell C. Actin-filled nuclear invaginations indicate degree of cell de-differentiation. Differentiation 2003;71:414–424. [PubMed: 12969334]

Kim YB, Yu J, Lee SY, Lee MS, Ko SG, Ye SK, Jong HS, Kim TY, Bang YJ, Lee JW. Cell adhesion status-dependent histone acetylation is regulated through intracellular contractility-related signaling activities. J Biol Chem 2005;280:28357–28364. [PubMed: 15961394]

Lammerding J, Schulze PC, Takahashi T, Kozlov S, Sullivan T, Kamm RD, Stewart CL, Lee RT. Lamin A/C deficiency causes defective nuclear mechanics and mechanotransduction. J Clin Invest 2004;113:370–378. [PubMed: 14755334]

Langevin HM, Bouffard NA, Badger GJ, Iatridis JC, Howe AK. Dynamic fibroblast cytoskeletal response to subcutaneous tissue stretch ex vivo and in vivo. Am J Physiol Cell Physiol 2005;288:C747–756. [PubMed: 15496476]

Langevin HM, Cornbrooks CJ, Taatjes DJ. Fibroblasts form a body-wide cellular network. Histochem Cell Biol 2004;122:7–15. [PubMed: 15221410]

Langevin HM, Storch KN, Cipolla MJ, White SL, Buttolph TR, Taatjes DJ. Fibroblast spreading induced by connective tissue stretch involves intracellular redistribution of alpha- and beta-actin. Histochem Cell Biol 2006;125:487–495. [PubMed: 16416024]

Mandadapu KK, Govindjee S, Mofrad MR. On the cytoskeleton and soft glassy rheology. J Biomech 2008;41:1467–1478. [PubMed: 18402964]

Maniotis AJ, Chen CS, Ingber DE. Demonstration of mechanical connections between integrins, cytoskeletal filaments, and nucleoplasm that stabilize nuclear structure. Proc Natl Acad Sci U S A 1997;94:849–854. [PubMed: 9023345]

McBeath R, Pirone DM, Nelson CM, Bhadriraju K, Chen CS. Cell shape, cytoskeletal tension, and RhoA regulate stem cell lineage commitment. Dev Cell 2004;6:483–495. [PubMed: 15068789]

Philip JT, Dahl KN. Nuclear mechanotransduction: response of the lamina to extracellular stress with implications in aging. J Biomech 2008;41:3164–3170. [PubMed: 18945430]

Pratt, WK. Digital Image Processing. John Wiley & Sons; NY: 1991. p. 636-644.

Ridley AJ, Hall A. The small GTP-binding protein rho regulates the assembly of focal adhesions and actin stress fibers in response to growth factors. Cell 1992;70:389–399. [PubMed: 1643657]

Ridley AJ, Paterson HF, Johnston CL, Diekmann D, Hall A. The small GTP-binding protein rac regulates growth factor-induced membrane ruffling. Cell 1992;70:401–410. [PubMed: 1643658]

Rowat AC, Lammerding J, Ipsen JH. Mechanical properties of the cell nucleus and the effect of emerin deficiency. Biophys J 2006;91:4649–4664. [PubMed: 16997877]

Storch KN, Taatjes DJ, Bouffard NA, Locknar S, Bishop NM, Langevin HM. Alpha smooth muscle actin distribution in cytoplasm and nuclear invaginations of connective tissue fibroblasts. Histochem Cell Biol 2007;127:523–530. [PubMed: 17310383]

Thomas CH, Collier JH, Sfeir CS, Healy KE. Engineering gene expression and protein synthesis by modulation of nuclear shape. Proc Natl Acad Sci U S A 2002;99:1972–1977. [PubMed: 11842191]

Vaziri A, Mofrad MR. Mechanics and deformation of the nucleus in micropipette aspiration experiment. J Biomech 2007;40:2053–2062. [PubMed: 17112531]

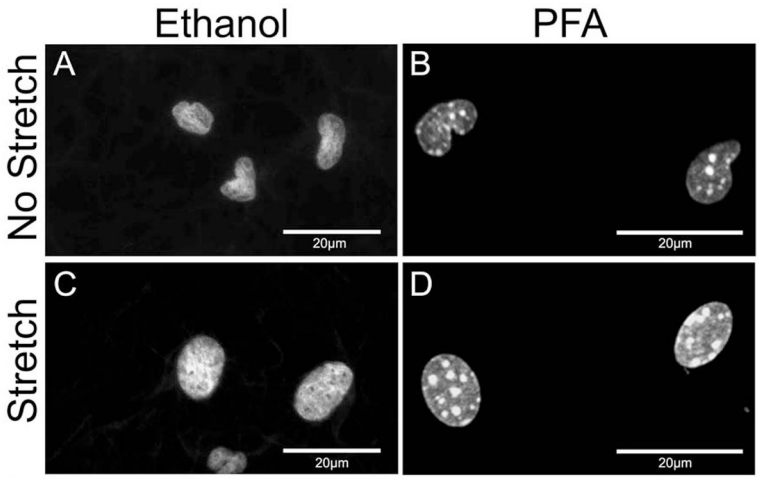

Fig. 1.

Morphological appearance of fibroblast nuclei in non-stretched and stretched mouse subcutaneous areolar connective tissue (30 minutes *ex vivo*) fixed with 95% ethanol (A,C) vs. 3% PFA(B,D) and stained with DAPI. Images are composite projections of stacks containing 20 optical sections taken at a 0.33 μm inter-image interval.

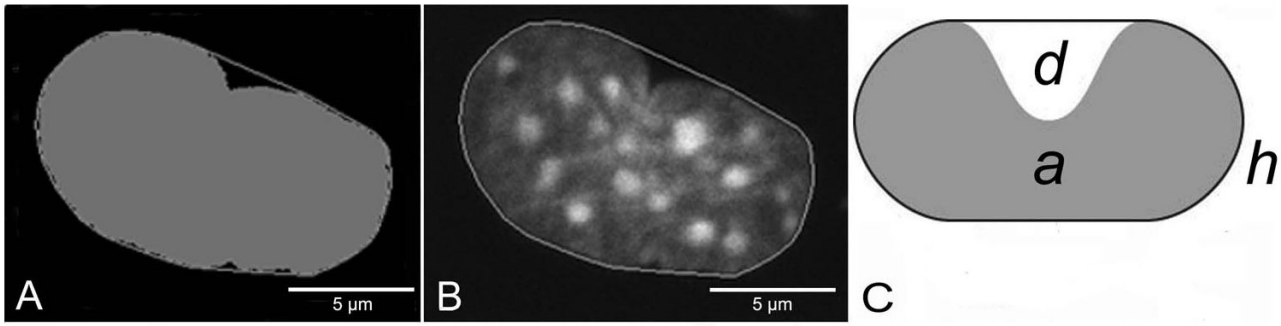

Fig. 2.

(A,B) Illustration of method used to analyze image stacks for nuclear cross sectional area *(*shaded area in A*)* and nuclear convex hull area (area inside line in A and B); (C) Schematic drawing of the areas used to compute the relative concavity. In panel C, *a* (gray region) represents nuclear cross sectional area; *h* represents the area of its convex hull (the interior of the dark contour); *d=h-a* (white region) represents the deficit and estimates the sum of invaginated areas.

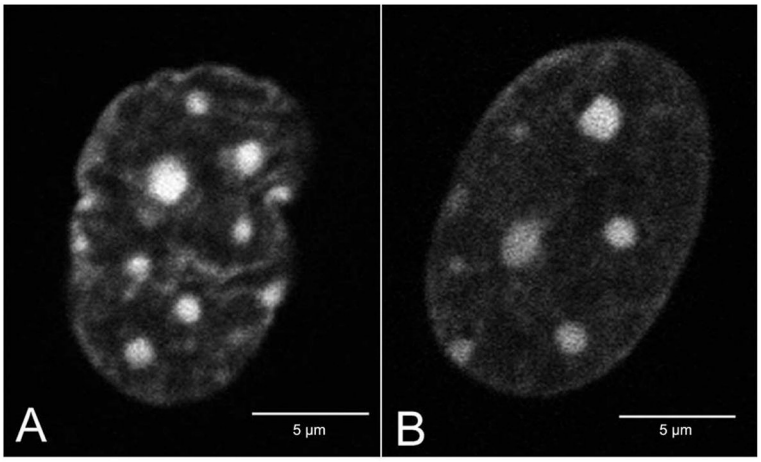

Fig. 3.

Example of high magnification image of fibroblast nuclei within non-stretched (A) and stretched (B) mouse subcutaneous areolar connective tissue (30 minutes *ex vivo*). Whole tissue samples were fixed in 3% PFA, stained with DAPI nucleic acid stain and imaged with confocal microscopy. Each image represents a single optical section of 0.7 μm thickness.

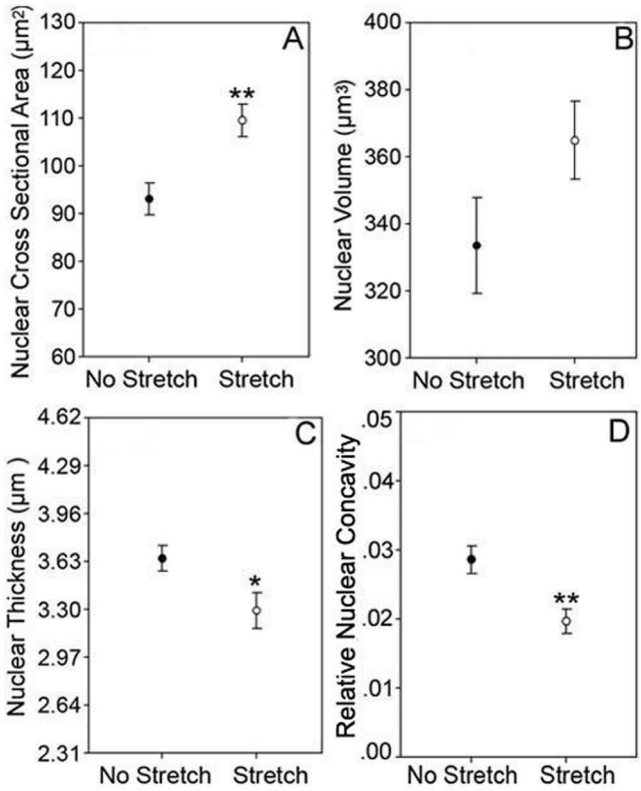

Fig. 4.

Morphometric analysis of the effect of tissue stretch (30 minutes *ex vivo*) on subcutaneous areolar connective tissue fibroblast nuclear shape: (A) nuclear cross sectional area, (B) nuclear volume, (C) nuclear thickness and (D) relative concavity. Tissue was fixed in 3% PFA. Closed circles indicate non-stretched samples and open circles indicate stretched samples. Error bars represent SEM. Significantly different from non-stretched: **p <.01, *p < .05 (ANOVA). For all graphs N = 28 mice (14 per condition).

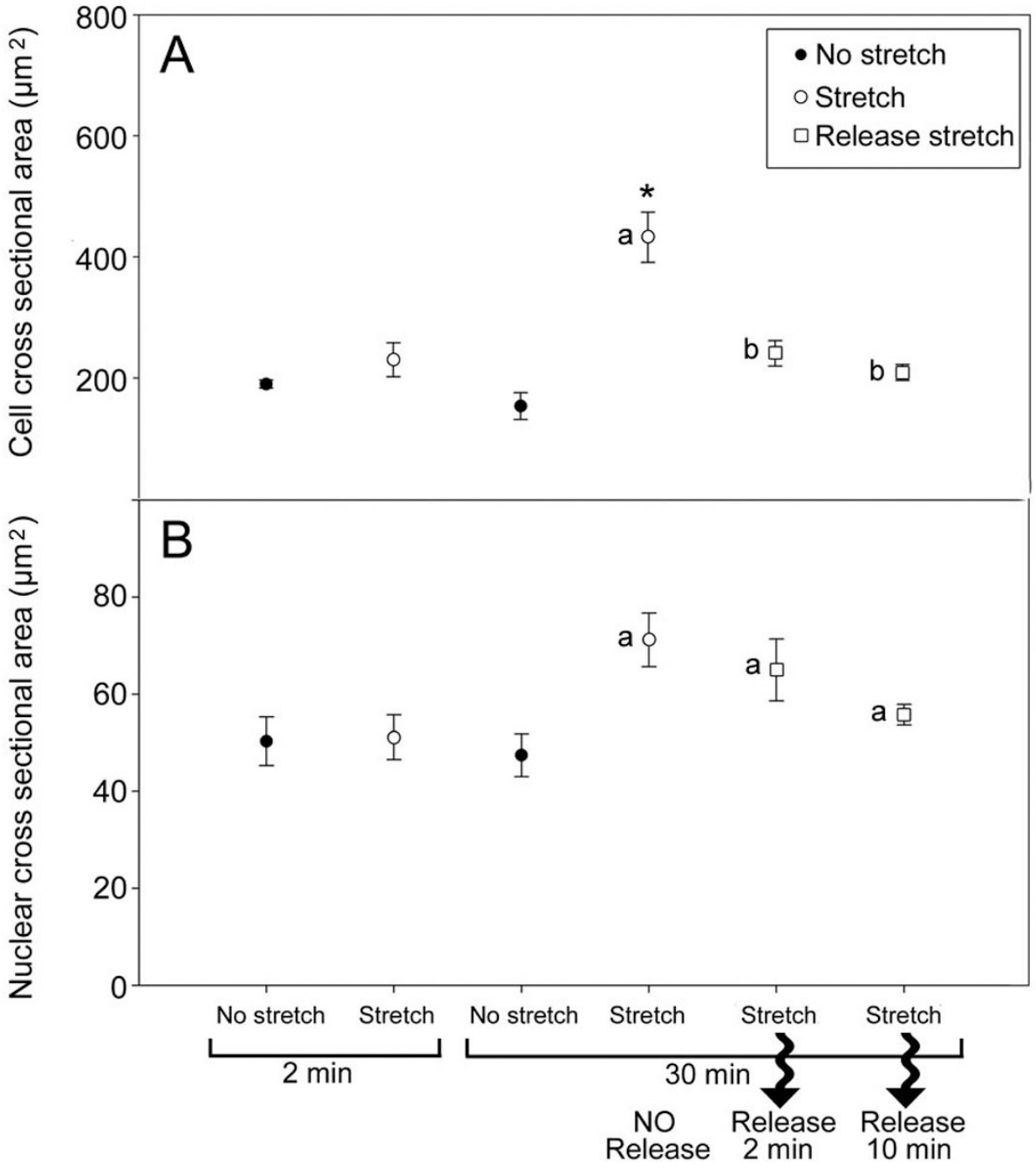

Fig. 5.

Effect of tissue stretch for 2 minutes vs. 30 minutes *ex vivo*, as well as following release of stretch for 2 minutes vs. 10 minutes on cell cross sectional area (A) and nuclear cross sectional area (B). Tissue samples were fixed in 95% ethanol. Error bars represent SEM. *Significantly different from non-stretched ($p < .05$ paired t-test). Means sharing a common letter are not significantly different (Fisher's LSD, $p<.05$). N = 12 mice (3 per condition).

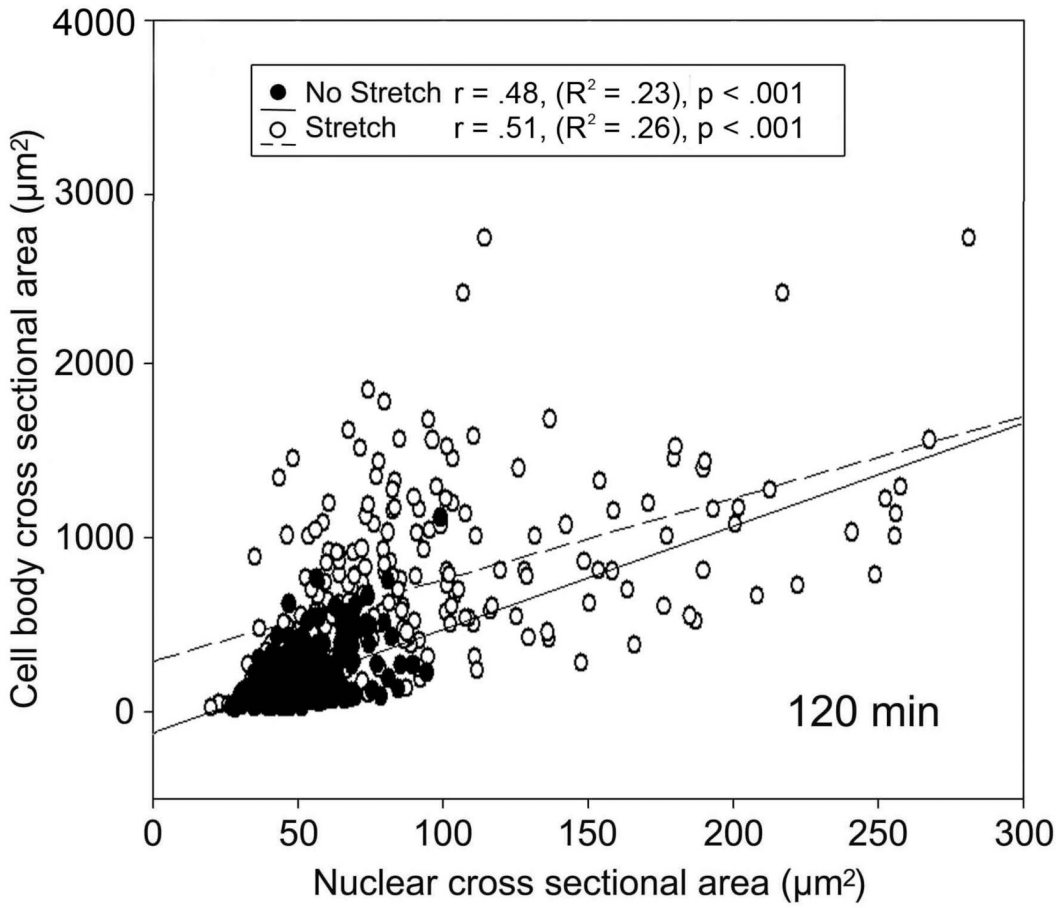

Fig. 6.

Relationship between fibroblast cell body cross sectional and nuclear cross sectional area in stretched and non-stretched tissue incubated for 120 minutes. Circles indicate individual cells in stretched (open circles) and non-stretched (closed circles) tissue. Linear regression lines are shown for stretched (dashed lines) and non-stretched (solid lines) tissue samples.

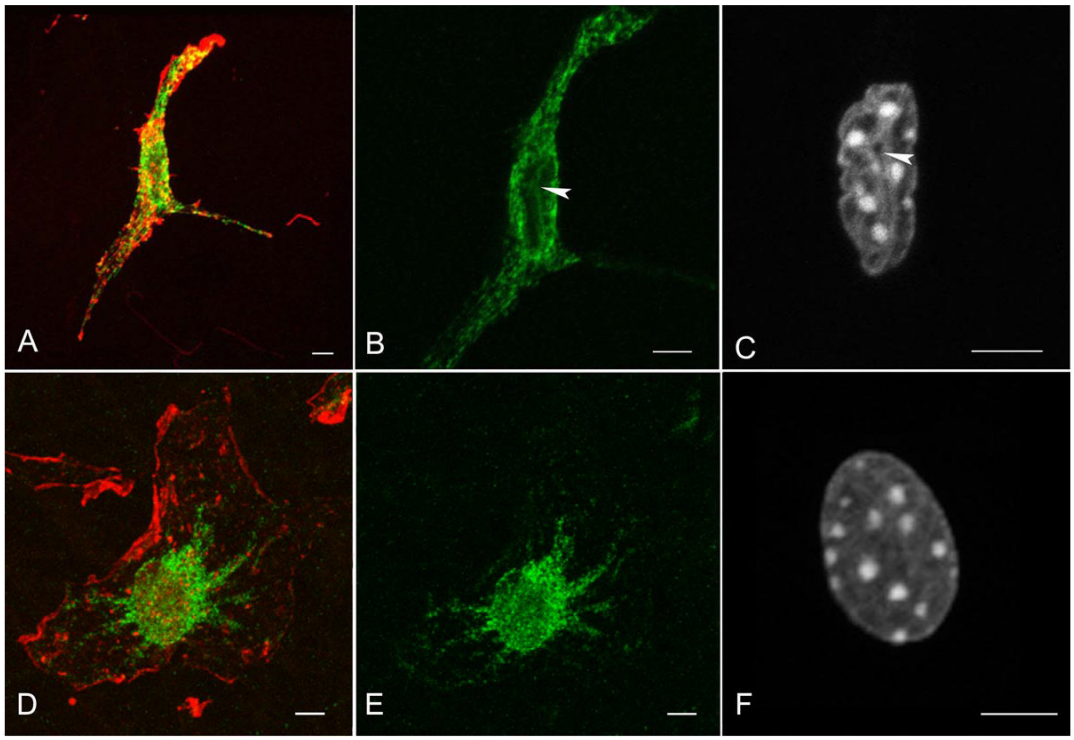

Fig. 7.

Fibroblasts within non-stretched (*A,B,C*) and stretched (*D,E,F*) mouse subcutaneous areolar connective tissue (30 minutes *ex vivo*) stained with phalloidin (*red, A,D*), immunohistochemical staining for α-actin (*green, A,B,D,E*) and DAPI nucleic acid stain (*white, C,F*) imaged with confocal laser scanning microscopy using a PlanApochromat 63× (NA=1.4) oil immersion lens. Arrowheads (*B,C*) indicate a nuclear invagination containing α-actin. Images are projections of eight optical sections. *Scale bars* 5 μm.

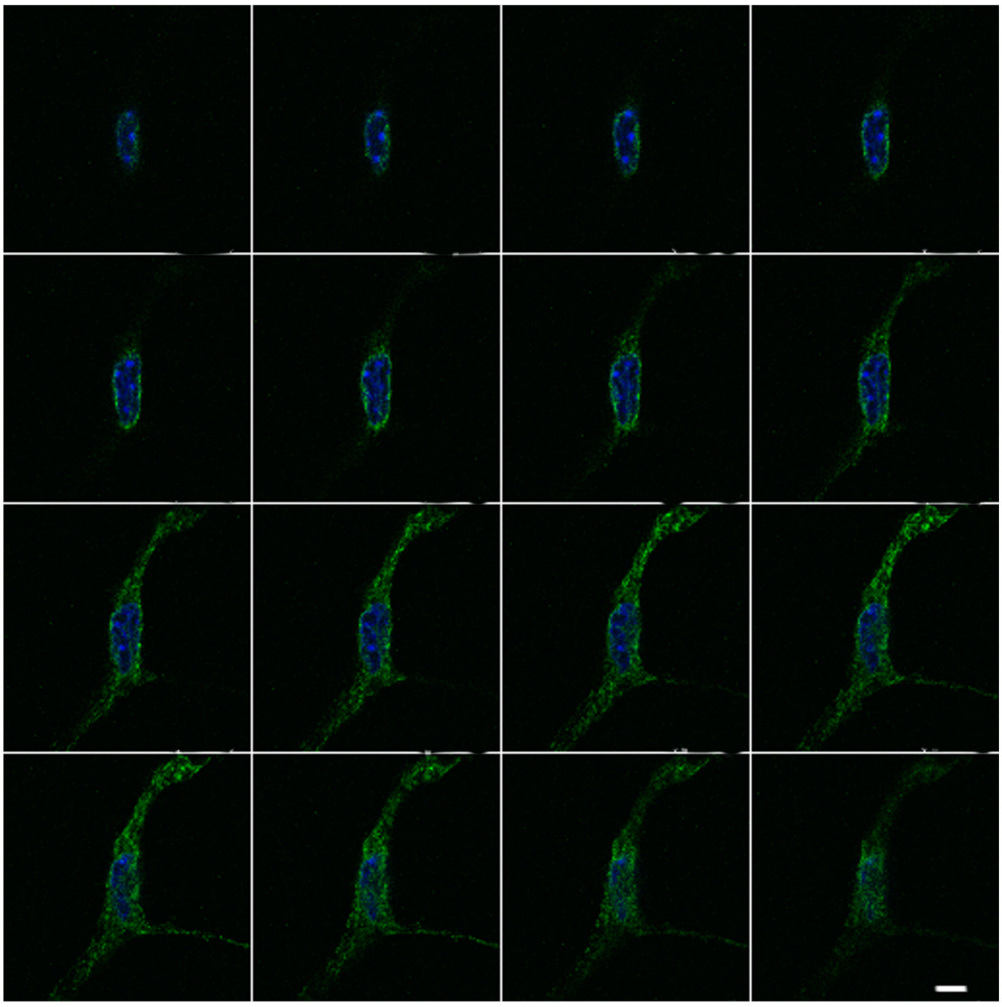

Fig. 8.
Serial confocal microscopy images showing a fibroblast within non-stretched mouse subcutaneous areolar connective tissue (30 minutes *ex vivo*) stained for α-actin (green) and DAPI (blue). The middle two rows of optical sections shows presence of α-actin positive staining in nuclear invaginations within the nuclear domain. Optical sections represent a 0.33 μm inter-image interval. *Scale bar* 5 μm.

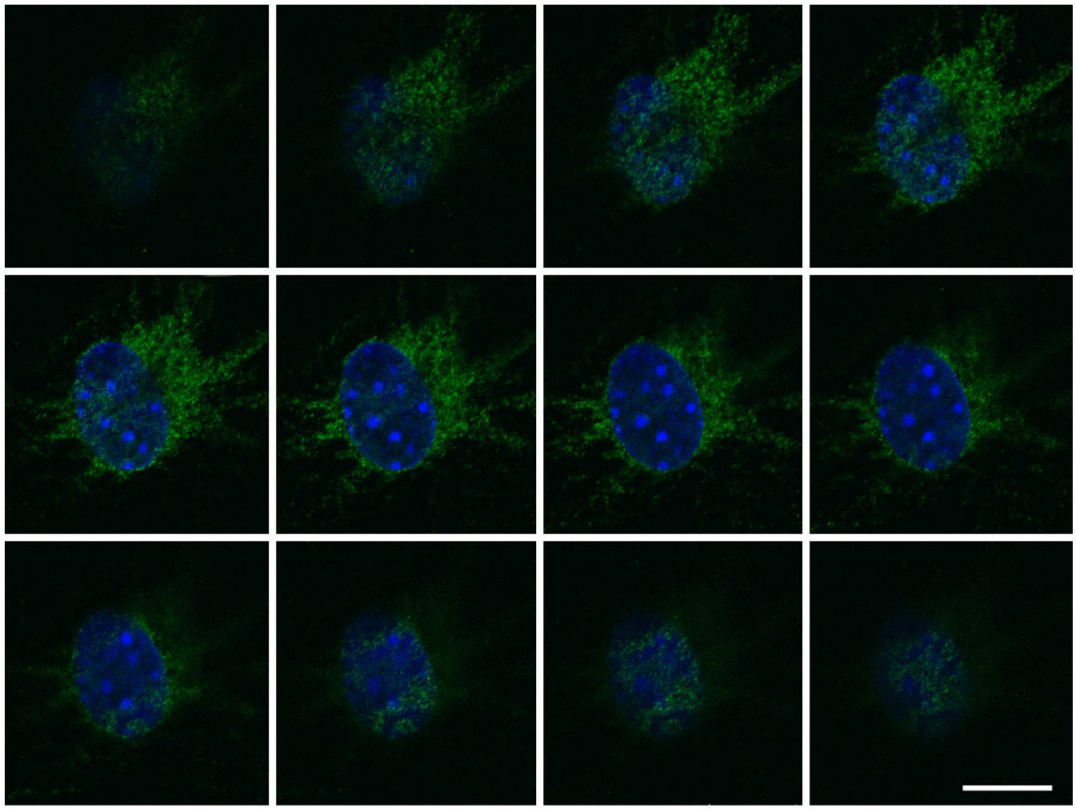

Fig. 9.
Serial confocal microscopy images showing a fibroblast within stretched mouse subcutaneous areolar connective tissue (30 minutes *ex vivo*) stained for α-actin (green) and DAPI (blue). The middle row of optical sections shows the absence of α-actin positive staining in the nuclear domain. Optical sections represent a 0.33 μm inter-image interval. *Scale bar* 5 μm.

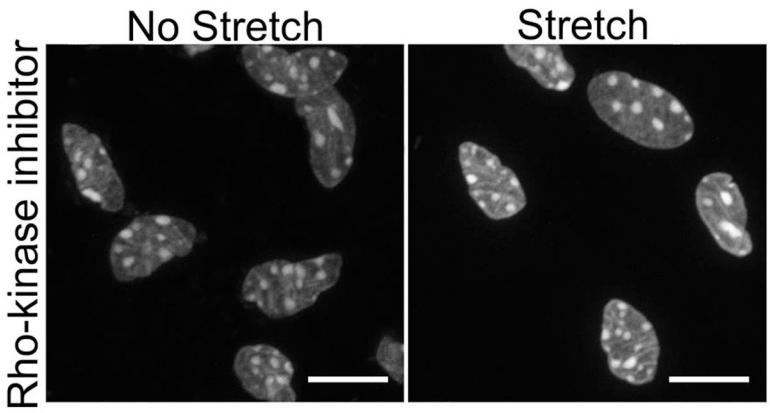

Fig. 10.

Fibroblast nuclear morphology in mouse subcutaneous areolar connective tissue incubated ex vivo for 30 minutes with and without stretch in the presence of an inhibitor of Rho kinase. Mean±SE nuclear cross sectional area was 74.6±9.5 μ^2 with stretch and 77.4±5.4 μ^2 without stretch (based on N=11-14 cells per condition). Scale bars, 10μm.